



Organic aerosol enhances boreal forest photosynthesis under cumulus clouds



Ekaterina Ezhova ¹, Aino Aarne¹, Antti Arola ², Antti Lipponen ², Anna Lintunen¹, Harri Kokkola ^{2,3}, Ilona Ylivinkka ¹, Taina Yli-Juuti ³, Tuukka Petäjä ¹, Veli-Matti Kerminen ¹, Annele Virtanen ³ & Markku Kulmala ¹

Boreal forest is an important source of atmospheric aerosol particles, making clouds more reflective in a warmer climate. However, little is known about the aerosol effect on the scattering of radiation under a cloudy sky, which can have a cooling effect by enhancing the carbon uptake of boreal ecosystems. Here we show observational evidence that higher natural aerosol loadings associated with warmer conditions increase diffuse radiation in the presence of cumulus clouds and further invigorate photosynthesis in the boreal forest. The enhancement of photosynthesis occurs in the morning and evening or under clouds with cloud fraction 0.4–0.8, when moderate vapor pressure deficit keeps stomata in foliage open and the diffuse fertilization effect is maximized. The total effect of high aerosol loading is a further increase of the daily carbon uptake under cumulus clouds by 12% of the possible diffuse fertilization enhancement in the ecosystem. Our results provide observational support for the atmosphere-biosphere photosynthesis-based feedback not only under clear sky but also under cumulus clouds frequently observed over boreal forest in summer.

Boreal forests occupy 14% of the land area globally and play an important role in regional and global climate. The impact of boreal forests on the atmosphere is multifaceted and includes, besides carbon sequestration and storage, effects on the surface energy balance via albedo and surface roughness changes^{1,2}, on the water cycle via evapotranspiration^{3,4}, and on the aerosol population^{5–7}. Forest is a source of primary aerosol and volatile organic compounds participating in the formation and growth of secondary organic aerosol (OA) particles^{4,8}. Primary aerosol particles were estimated to contribute only about 10–20% of climatically relevant aerosol population in boreal forest⁹. Dominating secondary aerosol is tightly linked to temperature-dependent monoterpane emissions especially from coniferous forest species^{7,8}. Aerosol particles, water vapor, and turbulence are major factors controlling clouds' formation and dynamics. While the forests' impacts on clouds, including higher cloud fraction over forests compared to grassland^{10–12}, and increase in cloud condensation nuclei and clouds' albedo in response to aerosol loading^{13,14} were reported in satellite-based studies and studies utilizing global models^{15–17}, the observed regional albedo effect was not reproduced by global models¹⁸. In addition to reflecting, clouds scatter radiation and may increase its diffuse fraction. The enhancing effects of diffuse radiation on forest photosynthesis have been reported in many observational and modeling studies^{19–23}. For example, Ezhova et al. found that the largest increase in photosynthesis of

several forest ecosystems occurs under cloudy skies¹⁹. They also quantified the effect of aerosol loading on radiation and photosynthesis under clear sky; however, they did not separate between types of clouds, and did not consider the effect of aerosol loading under cloudy sky. In addition, up to date, there have been only few Earth System Model-based studies focusing on the effect of temperature increase on aerosol population and further on clouds, diffuse radiation, and photosynthesis^{24,25}, and these studies reported contrasting results. Here we provide the first fully observational evidence of the aerosol-driven enhancement of diffuse radiation under cloudy sky, and further quantify the effect on boreal forest photosynthesis using a long-term data set. Furthermore, we estimate the strength of the negative climate feedback due to aerosol-radiation-photosynthesis interactions in a warming climate^{26–28}.

The in-situ data set is from the flagship station SMEAR II (Station for Measuring Earth surface- Atmosphere Relations²⁹) at Hytylä in southern Finland. Here we worked with 1-h average values of different in-situ parameters (Methods) focusing on clouds' and aerosol particles' effect on solar radiation and boreal ecosystem photosynthesis during the summer months July–August. Aerosol particles affect diffuse radiation in two ways, directly affecting the radiative transfer and indirectly by modifying the optical properties of clouds, and here we consider cloudy sky, meaning both these effects in action. First, we studied how aerosol loading influences

¹Institute for Atmospheric and Earth System Research, University of Helsinki, Helsinki, Finland. ²Atmospheric Research Centre of Eastern Finland, Finnish Meteorological Institute, Kuopio, Finland. ³Department of Technical Physics, University of Eastern Finland, Kuopio, Finland.

e-mail: ekaterina.ezhova@helsinki.fi

diffuse radiation under a cloudy sky, and second, what effect the change in diffuse radiation has on ecosystem photosynthesis.

As different weather systems, each with its own dynamics, favor different clouds, we separated the data by cloud type³⁰ and focused only on cumulus clouds. Cumulus clouds were chosen because they are known to enhance photosynthesis²¹ and because they are frequent during the growing season in boreal region^{30,31}. At SMEAR II, cumulus clouds represent 20–30% of all sky conditions during summer daytime, being the second dominating type of clouds after stratus with 25–30%³⁰. In addition, continental cumulus clouds follow a typical diurnal development cycle, directly interacting with the underlying surface via an air mass in which they form. Furthermore, as we were interested in aerosol-driven change in diffuse radiation, we followed Yli-Juuti et al. approach¹³ and separated two distinct cases with low and high OA loading (Methods), with the low-aerosol case corresponding to the OA mass loading below $1.59 \mu\text{g m}^{-3}$ (the lowest 33 percentile values) and high aerosol case to the loading above $3.02 \mu\text{g m}^{-3}$ (the highest 33 percentile values). The choice of OA mass as the variable linked to radiation scattering at SMEAR II site is justified by several previous studies. Heikkilä et al.³² showed that during summer months, particulate matter smaller than 1 micron, PM_1 , is clearly dominated by organics (>80% in total PM_1), whereas Petäjä et al. demonstrated an increase of OA mass in summer linked to a simultaneous increase of in-situ and above-ground measured scattering and backscattering coefficients¹⁴. Biogenic origin of OA at SMEAR II is confirmed in previous studies by correlations of OA mass with temperature and aerosol yields from monoterpene emissions along air mass trajectories^{8,13}. Data analyses are described in detail in Methods.

Results and discussion

Aerosol and clouds effect on diffuse radiation

As expected, the level of diffuse radiation increased when cloud fraction (CF) increased (Fig. 1a) because cumulus clouds scatter radiation efficiently²¹, and larger CF indicates more clouds. However, this general increase is modulated by aerosol loading as shown in Fig. 1a. At the lowest CF, median diffuse radiation was ~50% higher for large OA than for low OA. Interestingly, the aerosol effect remains noticeable even under larger CF, although decreasing from 50% to about 15% under the almost overcast sky (Fig. 1a).

A similar effect was observed if binning was done using the time of the day (Fig. 1b). The general pattern was that diffuse radiation increases towards the middle of the day, remaining low in the morning and evening

hours³³. In the early morning and late afternoon, the difference in diffuse radiation between low and high OA is not statistically significant. However, at 8:00–10:00 local time (LT) this difference becomes large (90 W/m^2 , i.e., 50% larger under high than under low aerosol load) and remains statistically significant throughout the day. The substantial morning difference in diffuse radiation can be important for photosynthesis because atmospheric humidity, which might be a limiting factor in the afternoon on a warm summer day, is sufficient in the morning.

The diffuse radiation difference between the high and low aerosol conditions in Fig. 1a could be related to the diurnal pattern of the solar zenith angle, whereas the corresponding difference in Fig. 1b could be associated with different cloud fractions. Supplementary Fig. 1 shows zenith angle distributions corresponding to the bins in Fig. 1a and CF distributions related to Fig. 1b. According to Supplementary Fig. 1a, high aerosol conditions have in general lower solar zenith angles. This is the consequence of sampling (Supplementary Fig. 2): high OA is typically observed on warm days, and it is in general warmer in July than in August. Thus, high aerosol conditions are overrepresented in July compared to August. Hence, we need to introduce corrections to the radiation difference associated with the zenith angle. We used a simple clear sky model of diffuse radiation³³ (Methods) and Supplementary Fig. 3, to show that the corrections for the lowest CF bin do not exceed 25%. Note that the model uses aerosol optical depth (AOD_{675}) as aerosol-related variable, and Supplementary Fig. 3a shows a statistically significant moderate correlation between OA mass and AOD_{675} . Interestingly, the clear sky model gives median value of diffuse radiation close to 84 W/m^2 under low aerosol conditions and 135 W/m^2 under high aerosol conditions (Supplementary Fig. 3b). This is about 30–40 W/m^2 less than the median values in Fig. 1a (115 and 175 W/m^2 , respectively), thus 25–30% of diffuse radiation at the lowest CF could be due to clouds. However, the difference between the two values, modeled (135 – 84 W/m^2 and measured (175 – 115 W/m^2), is almost the same suggesting that direct aerosol effect could be a viable explanation for the differences at least at the lowest CF.

The difference in CF between the low and high aerosol conditions does not show any consistent diurnal pattern (Supplementary Fig. 1b), and most often is not statistically significant, so CF cannot be responsible for the significant differences found in the diffuse radiation levels between the low and high aerosol loads. However, there is also a difference in solar zenith angles (Supplementary Fig. 4a), which are again lower for the higher aerosol conditions, meaning higher top-of-atmosphere radiation, and hence,

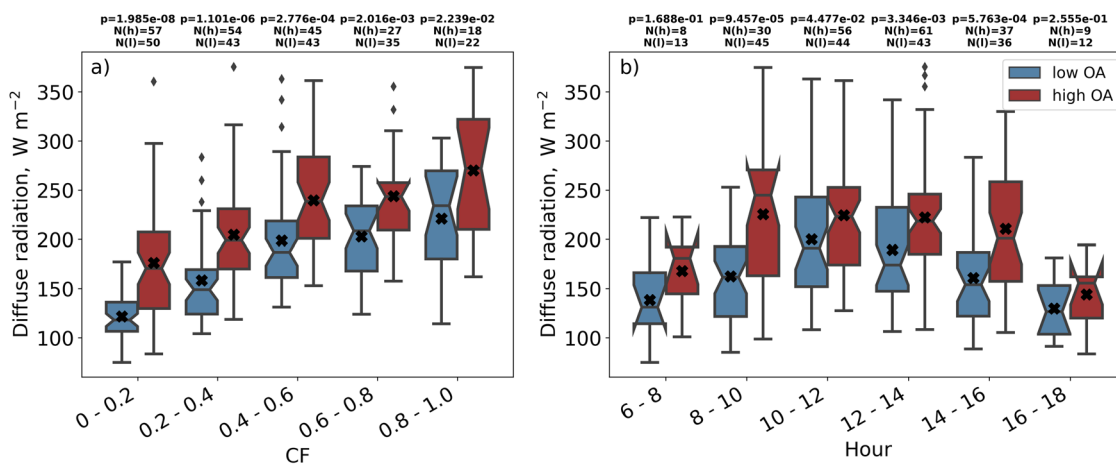


Fig. 1 | Effect of aerosol and clouds on diffuse radiation. Diffuse radiation as a function of cloud fraction (a) and time of the day (b). Blue notched boxes show median values and interquartile ranges (IQR, 25–75 percentile) of diffuse radiation under low organic aerosol (OA) loading, and red notched boxes - under high OA loading. Whiskers denote 1.5 IQR range, and the remaining points are ‘outliers’. Black crosses show mean values. Results testing the difference in diffuse radiation between the low and high OA loading cases (p -values, Wilcoxon rank sum test) at

each cloud fraction bin or time of the day, as well as the number of points for low and high aerosol cases ($N(l)$ and $N(h)$, respectively) are shown above the figures. In panel (a), low and high OA observations are statistically significantly different from each other in all the bins ($p < 0.05$), and the same is true for the panel (b), except for the earliest and latest hour bins (6:00–8:00 and 16:00–18:00 LT), where the difference is not statistically significant.

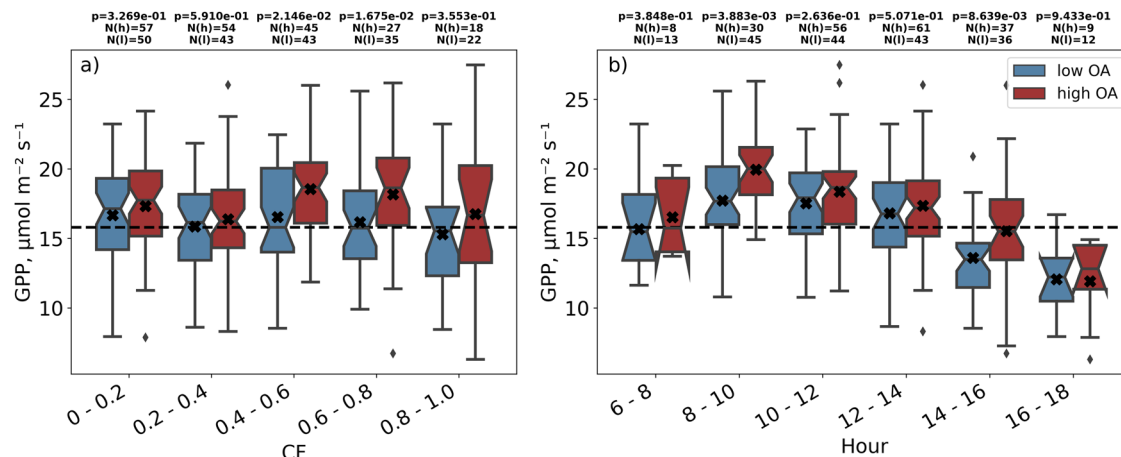


Fig. 2 | Effect of aerosol and clouds on photosynthesis. GPP as a function of cloud fraction (a) and time of the day (b). Blue notched boxes show median values and interquartile ranges (IQR, 25–75 percentile) of GPP under low OA loading, and red notched boxes - under high OA loading. Whiskers denote 1.5 IQR range, and the remaining points are ‘outliers’. Black crosses show mean values. The dashed lines mark mean GPP on a clear sky day with low aerosol loading. Results testing the

difference in GPP between the low and high aerosol load cases (*p*-values, Wilcoxon rank sum test) at each cloud fraction bin or time of the day, as well as the number of points for low and high aerosol cases (*N*(l) and *N*(h), respectively) are shown above the figures. In the left panel, only the GPP difference at CF 0.4–0.8 is statistically significant, and in the right panel, only the GPP difference at hours at 8:00–10:00 and 14:00–16:00 LT is statistically significant.

possibly higher global and diffuse radiation. Also in this case, however, the corrections on the zenith angle cannot explain more than 15% of the diffuse radiation difference (Supplementary Fig. 3).

Related to scattering, it can also be insightful to look at the diffuse fraction, i.e., the ratio of diffuse to global radiation. Supplementary Fig. 5a shows that the median diffuse fraction increases with an increasing CF, as expected, from 0.2 under low CF to about 0.7 under high CF. Interestingly, the diffuse fraction is about 0.1 larger for high aerosol conditions at all CFs except for the highest one, confirming that high aerosol conditions induce more scattering. Looking at the diurnal cycle, especially for 08:00–10:00 LT, it follows from Supplementary Fig. 5b that the diffuse fraction is larger under high OA, about 0.5 compared to 0.4 for low OA. After 10:00 LT, the difference in the diffuse fraction is not statistically significant. Note that the median levels of the diffuse fraction are close to 0.4–0.5 all day, which has shown to be the optimum for boreal forest ecosystems’ photosynthesis^{19,34}.

So why does higher aerosol loading induce higher diffuse radiation? To elucidate the mechanisms behind the difference observed in Fig. 1, we note that aerosol particles can influence diffuse radiation either via direct scattering of solar radiation or indirectly, via interaction with clouds. The effect of larger aerosol loading on diffuse radiation, i.e., direct effect, is important under low CF but can be expected to be diminishing or negligible in the presence of cumulus clouds. The indirect effect of aerosol loading over forests on clouds and further on diffuse radiation has not been quantified, although globally indirect effect is estimated to be stronger than direct one³⁵. Our finding that higher OA increases diffuse radiation for all cloud fractions emphasizes the role of aerosol particles for enhancement of diffuse radiation not only under clear sky (direct effect) but also under clouds (direct and indirect effects).

Aerosol and clouds effect on photosynthesis

Sufficient global radiation, accompanied by enhanced diffuse radiation cause higher light use efficiency at the ecosystem level and boost photosynthesis^{19–23}. For this reason, cumulus clouds with transmittance of about 80%³⁰ and yet high diffuse radiation level, are considered favorable for photosynthesis²¹. Here we study what effect cumulus clouds and different aerosol loadings, associated with the radiation regimes discussed in the previous section (Fig. 1, Supplementary Fig. 5), have on the ecosystem photosynthesis represented by gross primary production (GPP).

With the threshold value³⁶ of about 350 W/m², the level of global radiation is not limiting for photosynthesis at CF from 0.0 to 0.8 (Supplementary Fig. 6a), and during the day from 8:00 to 16:00 LT (Supplementary

Fig. 6b); thus, GPP can be enhanced if the diffuse radiation level is sufficiently high. To quantify GPP enhancement, we take 15.8 $\mu\text{mol m}^{-2} \text{s}^{-1}$ as a reference value (corresponding to the mean midday GPP value at SMEAR II under clear sky and low OA¹⁹). In Fig. 2a, we can see that the median GPP value at the low OA is close to this reference value for all CF. However, for high OA and CF between 0.4–0.8, even 25th percentile is higher than 15.8 $\mu\text{mol m}^{-2} \text{s}^{-1}$, indicating enhanced photosynthesis. Related to the diurnal cycle, at low OA, photosynthesis is higher than the mean midday value under clear sky from 8:00 to 14:00 LT and at high OA, from 8:00 to 16:00 LT (Fig. 2b).

Comparing low and high aerosol cases around midday, we see that the GPP difference is not statistically significant (Fig. 2b). It is significant, remarkably, only between 8:00–10:00 and 14:00–16:00 LT, which correspond also to the largest diffuse radiation differences (Fig. 1b). Especially in the morning, the median GPP value is 20 $\mu\text{mol m}^{-2} \text{s}^{-1}$, which is about 30% higher than the reference value. In the afternoon, median GPP values fall below the reference level under low OA but are still near the reference value under high OA.

Non-significant GPP differences between low and high OA conditions in the middle of the day and at the lowest CF suggest that factors other than the radiation alone are important. In summer, vapor pressure deficit (VPD) influences photosynthesis via stomatal control^{36,37}. Therefore, we compare temperature and VPD between low and high OA conditions (Supplementary Figs. 7, 8). Air temperature is higher under high OA for all CF, but especially for low CF (6–7 °C difference between the low and high OA cases for CF 0.0–0.4 vs 3–4 °C for CF 0.6–0.8). Also, under low CF and high OA conditions, the median temperatures that are reached are about 23–24 °C, whereas upper 1.5 IQR value approaches 30 °C. The median temperatures under low aerosol conditions are much milder, fluctuating at about 17 °C for all but the highest CF. It is therefore possible that the effect of higher diffuse radiation at high OA and low CF is compensated by the stomatal response to high temperatures. At SMEAR II, the value of VPD when GPP starts to decrease is about 1 kPa³⁶. From Supplementary Fig. 8a, 75% of VPD values under high OA are larger than 1 kPa for CF between 0.0 and 0.6, implying that GPP can indeed be reduced due to the VPD effect in these conditions. At lower OA, most of the VPD values are lower than 1 kPa, meaning that VPD should not be limiting photosynthesis during low OA. As expected, the highest values of VPD irrespective of aerosol loading are reached at the lowest cloud fractions.

When looking at the diurnal cycle (Supplementary Figs. 7b, 8b), we see a similar pattern: the temperature and VPD are significantly higher for large

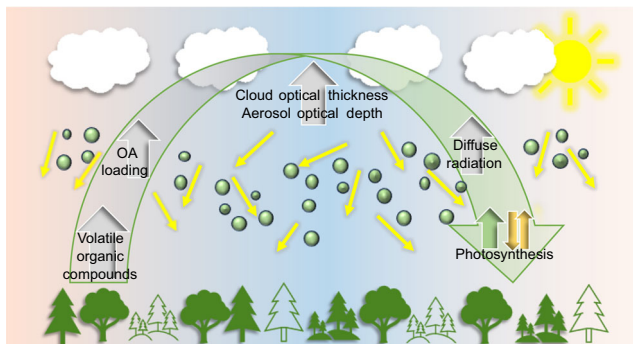


Fig. 3 | Linking forests and clouds. Big green arrow shows the direction of interactions, and smaller gray arrows indicate direction of the change in the variables due to the interactions. In a warmer climate, an increase in temperature leads to an increase in volatile organic compound emissions and organic aerosol loading, as well as an increase in aerosol optical depth. Aerosol particles and cumulus clouds enhance diffuse radiation and boost photosynthesis (green arrow); however, in water-limited conditions, this effect is less pronounced and can even be reversed (orange arrows in both directions).

OA during daytime with especially large VPD difference from 12:00 to 14:00 LT. The VPD difference is not statistically significant in the morning nor in the afternoon when the difference in the diffuse radiation is high and when GPP difference is significant. Especially in the morning, VPD for both high and low OA conditions is mostly below 1 kPa, making this time especially favorable for photosynthesis.

Part of the observed GPP difference between high and low OA could be due to the sampling: high OA was observed more often in July than in August, which could affect photosynthesis. To approximate a seasonal change of GPP, we used median GPP values during each day and fitted a curve to their median interannual values. We found that GPP decreased around mid-August (Supplementary Fig. 2). Our estimates point that about $1.2 \mu\text{mol m}^{-2} \text{s}^{-1}$, i.e. close to half of the largest differences in GPP shown in Fig. 2 could be due to this seasonality effect, which is most likely the consequence of the change in leaf area index (Methods).

Figure 2 suggests larger enhancement of photosynthesis related to increase in diffuse radiation above 200 W/m^2 both for CF and diurnal cycle. Previous analysis suggests that the absolute amount of diffuse radiation describes best the enhancement of photosynthesis, which was demonstrated for ecosystem, shoot and forest floor vegetation levels at SMEAR II²³. Under low and high OA, the amounts of diffuse radiation are clearly different. Under low OA, an increase in absolute diffuse radiation when CF changes from 0.2–0.4 to 0.4–0.6 is from $130\text{--}170 \text{ W/m}^2$ to $160\text{--}210 \text{ W/m}^2$; whereas under high OA, it is from $170\text{--}225 \text{ W/m}^2$ to $200\text{--}270 \text{ W/m}^2$, and it remains similarly high at CF 0.6–0.8. So an increase of diffuse radiation within $130\text{--}200 \text{ W/m}^2$ seems not so beneficial for photosynthesis as conditions with diffuse radiation above 200 W/m^2 , confirming that absolute amount of diffuse radiation is a relevant factor for photosynthesis in this ecosystem (see also Supplementary Fig. 9).

All in all, our analysis shows that high OA contributes to enhancement of photosynthesis under cloudy conditions, especially in the morning hours, 8:00–10:00 LT. Considering the cloud fraction, the best conditions for the photosynthesis are found under high OA and in the CF interval from 0.4 to 0.8. This is due to the combination of several factors: 1) high enough global radiation; 2) enhanced diffuse radiation, and 3) moderate vapor pressure deficit. Under these optimal conditions, GPP can be enhanced by up to 20% compared to the reference daytime GPP level under clear sky and low aerosol loading when seasonal effect due to sampling is accounted for.

Conclusions

We showed that higher aerosol loading under cumulus clouds leads to higher diffuse radiation (Fig. 3) but at the same time is associated with higher

vapor pressure deficit. Therefore, the enhancement in photosynthesis due to aerosol loading is observed in the morning and evening hours or at higher cloud fractions, when VPD effect is moderate. The morning enhancement is about 20% if compared to the mean GPP under clear sky and low aerosol loading, close to the highest (mean plus standard deviation) possible GPP values for this ecosystem¹⁹, and in line with the Large Eddy Simulations of a canopy with different leaf area indices²¹ finding a similar increase in carbon uptake in the morning hours compared to the clear sky values.

In addition to the enhancement of photosynthesis, our findings are in line with results, suggesting more reflective clouds under high aerosol conditions^{13,15}. Indeed, despite the large statistically significant difference in radiation at the top of the atmosphere between the cases with low and high aerosol loadings, the difference in global radiation at the surface is almost always insignificant, emphasizing the cooling role of aerosol particles.

Our results suggest an increase of photosynthesis under cumulus clouds when high aerosol loading is compared to low aerosol loading: about 6% in the morning and afternoon hours, and 1.2% over the whole day (Methods). These are non-negligible numbers for this ecosystem: the daily photosynthesis increase due to high aerosol loading under cumulus clouds is therefore at 12% of its maximum possible increase (Methods). Accounting for previous results, in a warmer climate, on clear days and days with cumulus clouds, boreal forest photosynthesis will be enhanced due to aerosol particles for the ecosystems with closed canopy similar to SMEAR II. The enhancement is 1.2–6.0% compared to respective photosynthesis values under low aerosol loading (6% is the clear sky value¹⁹) or 12–55% of the possible average photosynthesis increase due to diffuse fertilization. Our results support the concepts of COntinental Biosphere-Aerosol-Cloud-Climate feedback loop^{26–28} and CarbonSink³⁸: an enhancement of photosynthesis as a result of higher temperature causing increase in organic aerosol population. Estimates of the feedback, however, suggest that the negative radiative feedback due to photosynthesis enhancement under high aerosol loading is an order of magnitude weaker than the feedback due to clouds brightening¹³ (-0.01 vs $-0.1 \text{ W m}^{-2} \text{ °C}^{-1}$, see Methods). Furthermore, they provide support to the modeling results of biological volatile organic compounds (BVOC)-based atmosphere-biosphere feedback²⁵ and an increase in the GPP under cumulus clouds is similar to the numbers reported in the modeling study for boreal ecosystems (Methods). At the same time, our findings suggest that some Earth System Models are likely not sensitive enough to simulate this feedback²⁴.

Finally, it remains to be noted that the forest ecosystem at SMEAR II showed the smallest increase in GPP due to the diffuse radiation effect among the five stations considered in the previous study, whereas the largest increase was about 30% at hemiboreal sites in Estonia and Siberia¹⁹. Therefore, hemiboreal forest might be more sensitive to changes in aerosol loading potentially having a stronger increase in carbon uptake. These features need to be explored in more detail for a complete assessment of the feedback strength in different boreal ecosystems.

Methods

Site description and data sets

We used data from the SMEAR II station located at the Hyttiälä Forestry Field Station in southern Finland ($61^{\circ}50' \text{ N}$, $24^{\circ}17' \text{ E}$). The station is surrounded by a boreal coniferous forest dominated by 60-year-old Scots pine (*Pinus sylvestris* L.) trees of $\sim 20 \text{ m}$ height²⁹. The forest has a closed canopy.

Atmospheric observations from SMEAR II included data from seven summers for June–August of 2012–2018. The variables used included gross primary production (GPP), air temperature (T), relative humidity (RH), cloud base height (CBH), as well as global and diffuse radiation. Global and diffuse radiation were calculated from photosynthetically active radiation (PAR) and diffuse photosynthetically active radiation (diffPAR) by dividing these values by 2.06 (PAR quantum efficiency, as in Ezhova et al.¹⁹). Additionally, vapor pressure deficit (VPD) values were calculated using T and RH values in the

following way:

$$VPD = v_{ps} - v_{pa}, \quad (1)$$

where $v_{ps} = 611 \cdot \exp\left(\frac{17.27 \cdot T}{237.7 + T}\right)$ is the saturation water vapor pressure, and $v_{pa} = \frac{RH}{100} \cdot v_{ps}$ is the actual water vapor pressure. We also used lifting condensation level calculated using the algorithm provided in Romps³⁹.

All the aforementioned variables were downloaded from SmartS-MEAN website (<https://smear.avaa.csc.fi/>, last access 20.06.2024) with a temporal resolution of one minute, except for GPP, which had a temporal resolution of 30 min. Eddy-covariance method was used for measurements, and partitioning method of NEE to GPP and R, which is a combination of daytime and nighttime methods⁴⁰. Eddy-covariance based GPP require developed turbulence, so low-turbulence data are filtered out⁴¹. Besides uncertainties related to filtered data and partitioning, complex terrain and quickly changing meteorological conditions may cause changes in the fluxes, which cannot be attributed to any biotic or abiotic factors. All variables were averaged hourly, centered around exact hours.

Solar zenith angle was calculated using Matlab code implementing NREL solar position algorithm⁴². AOD₆₇₅ was downloaded from AERONET, site Hytytäla⁴³. Cloud fraction was calculated from the ceilometer data as the number of minutes per hour when cloud base was detected divided by 60.

Organic aerosol data was directly downloaded from Supplementary Material to Yli-Juuti et al.¹³ and the reader is referred to the above-mentioned study for measurements detail.

Cloud type classification

To differentiate between cloud types, we used the cloud classification algorithm by Ylivinkka et al.³⁰, which uses cloud base height and radiation-derived parameters transmittance (TR) and patchiness (PA) to classify clouds into seven different categories. Of these categories, we focused here on cumulus (Cu) clouds, as well as Clear sky+Cirrus. The temporal resolution of this data set was one minute, and we used it to find the prevailing cloud type for each hour. This was done by identifying the clouds which were present for at least 30 of the 60 classifications obtained during each hour. If Cu clouds were detected for more than 30 min during the hour, this hour was classified as Cu-dominated.

Splitting the data set into high and low aerosol loading cases

The data set was separated into days with high and low organic aerosol (OA) loading using the data provided in Yli-Juuti et al.¹³, where OA < 1.59 $\mu\text{g m}^{-3}$ were considered low and OA > 3.02 $\mu\text{g m}^{-3}$ were considered high, separation made using 33rd and 66th percentiles of the data, respectively. The OA data is composed of measurements taken in July and August over seven years, from 2012 to 2018.

The OA data was given in daily medians, which we used to distinguish between days with high and low OA loadings at SMEAR II. This data set was then restricted to cumulus clouds only. Furthermore, only the points for which the difference between lifting condensation level and cloud base height was less than 600 m were included to limit the data set to cumulus clouds which are coupled with the boundary layer.

Data binning by cloud fraction and diurnal cycle

To study the effect of OA mass loading on diffuse and global radiation, GPP, and VPD, the data was divided into bins corresponding to distinct values of cloud fraction (CF) and hours. The values of CF were divided into five evenly spaced intervals ranging between 0 and 1, whereas hours were divided into intervals of two hours between 6:00 and 18:00 local time. The Wilcoxon rank sum test was then used to look for statistically significant differences for the different variables in these intervals for days with high versus low OA mass loadings.

Estimates of diffuse radiation based on Solis model

According to the Solis model developed by Ineichen³³, the diffuse radiation can be modeled as follows:

$$I_{dh} = I'_0 \exp\left(-\frac{\tau_d}{\cos^d(SZA)}\right), \quad (2)$$

where I'_0 is the enhanced solar radiation (a function of aerosol optical depth at 700 nm, AOD₇₀₀, precipitable water w in [cm] and atmospheric pressure),

$$I'_0 = I_0 \left\{ I_{02} AOD_{700}^2 + I_{01} AOD_{700} + I_{00} + 0.071 \ln\left(\frac{p}{p_0}\right) \right\}, \quad (3)$$

with $I_{00} = 1.08 w^{0.0051}$, $I_{01} = 0.97 w^{0.032}$, $I_{02} = 0.12 w^{0.56}$, I_0 – solar constant, p_0 – atmospheric pressure at sea level;

$$\tau_d = t_{d4} \cdot AOD_{700}^4 + t_{d3} \cdot AOD_{700}^3 + t_{d2} \cdot AOD_{700}^2 + t_{d1} \cdot AOD_{700} + t_{d0} + t_{dp} \cdot \ln(p/p_0) \quad (4)$$

is the total diffuse optical depth and

$$d = 0.116 + 0.63 AOD_{700} - 0.337 AOD_{700}^2 + d_p \ln(p/p_0) \quad (5)$$

is the power of the cosine function, SZA is the solar zenith angle. As d_p is on the order of 0.01 at SMEAR II, and the level above sea is about 200 m, the pressure term is negligible.

The coefficients for τ_d are for $AOD_{700} < 0.05$:

$$t_{d4} = 86 \cdot w - 13800 \quad (6)$$

$$t_{d3} = -3.11 \cdot w + 79.4 \quad (7)$$

$$t_{d2} = -0.23 \cdot w + 74.8 \quad (8)$$

$$t_{d1} = 0.092 \cdot w - 8.86 \quad (9)$$

$$t_{d0} = 0.0042 \cdot w + 3.12 \quad (10)$$

$$t_{dp} = -0.83 \cdot (1 + AOD_{700})^{-17.2} \quad (11)$$

and for $AOD_{700} \geq 0.05$:

$$t_{d4} = -0.21 \cdot w + 11.6 \quad (12)$$

$$t_{d3} = 0.27 \cdot w - 20.7 \quad (13)$$

$$t_{d2} = -0.134 \cdot w + 15.5 \quad (14)$$

$$t_{d1} = 0.0554 \cdot w - 5.71 \quad (15)$$

$$t_{d0} = 0.0057 \cdot w + 2.94 \quad (16)$$

$$t_{dp} = -0.71 \cdot (1 + AOD_{700})^{-15.0}. \quad (17)$$

For calculations, we take AERONET values of AOD₆₇₅ instead of AOD₇₀₀ following Ezhova et al.¹⁹, and model diffuse radiation in the range of AOD₆₇₅ 0.01–0.20, which are close to high and low values at SMEAR II station, see Supplementary Fig. 3a; and SZA within 40°–65°, following typical values in Supplementary Figs. 1, 4.

We estimate the relative contributions of SZA and AOD from the contour plot (Supplementary Fig. 3b) using a linear approximation of the

function:

$$f(\text{SZA}, \text{AOD}) = f(\text{SZA}_0, \text{AOD}_0) + \frac{\partial f}{\partial \text{SZA}}(\text{SZA}_0, \text{AOD}_0)\Delta \text{SZA} + \frac{\partial f}{\partial \text{AOD}}(\text{SZA}_0, \text{AOD}_0)\Delta \text{AOD.} \quad (18)$$

The contributions of SZA and AOD can be estimated from Supplementary Fig. 3b as $\sim 10 \text{ W/m}^2$ and 30 W/m^2 respectively, leading to an estimate of 25% for the SZA contribution.

Effect of low-high OA sampling on photosynthesis

To estimate the effect of differential sampling on photosynthesis (Supplementary Fig. 2), we calculated weighted values of GPP for low and high aerosol:

$$\text{GPP}_{w,l(h)} = \frac{\sum_{i=1}^{62} \text{GPP}_i N_{i,l(h)}}{\sum_{i=1}^{62} N_{i,l(h)}}, \quad (19)$$

where $\text{GPP}_{w,l(h)}$ is the weighted value of maximum GPP for low (high) aerosol loading, GPP_i is the value of GPP on a given day (estimated from the curve), and $N_{i,l(h)}$ is the number of days with low (high) aerosol loading.

From this simple estimate, we can calculate $\text{GPP}_{w,l} = 16.9 \mu\text{mol s}^{-1} \text{ m}^{-2}$, and $\text{GPP}_{w,h} = 18.1 \mu\text{mol s}^{-1} \text{ m}^{-2}$. Therefore, the difference in sampling and seasonal change in photosynthesis can explain about $(18.1-16.9) = 1.2 \mu\text{mol s}^{-1} \text{ m}^{-2}$ out of obtained differences at low and high aerosol load, which is about 50% of the difference between median GPP values at CF 0.4–0.8 or morning (08:00–10:00). Indeed, at low aerosol loading, the morning median GPP value is $17.7 \mu\text{mol s}^{-1} \text{ m}^{-2}$, and at high aerosol loading, it is $20.0 \mu\text{mol s}^{-1} \text{ m}^{-2}$. The difference is $2.3 \mu\text{mol s}^{-1} \text{ m}^{-2}$, and the above-calculated value of $1.2 \mu\text{mol s}^{-1} \text{ m}^{-2}$ is about half of this value.

Daily mean estimates of GPP under cloudy sky

For future use and comparison, it is convenient to get the estimates of the mean daily GPP corrected to all summer season, June-August. Considering also June GPP, we got an estimate of mean value of median GPP during the day of $16.8 \mu\text{mol s}^{-1} \text{ m}^{-2}$. Considering that under low aerosol loading $\text{GPP}_{w,l} = 16.9 \mu\text{mol s}^{-1} \text{ m}^{-2}$, and under high aerosol loading, $\text{GPP}_{w,h} = 18.1 \mu\text{mol s}^{-1} \text{ m}^{-2}$, the values of GPP for low aerosol have to be corrected by $16.8-16.9 = -0.1 \mu\text{mol s}^{-1} \text{ m}^{-2}$ and for high aerosol – by $16.8-18.1 = -1.3 \mu\text{mol s}^{-1} \text{ m}^{-2}$ in order to be compared with the values for the full summer period.

We proceed with making estimates of GPP on cloudy days using Fig. 2b:

Time interval 8:00–16:00:

1. low aerosol loading, mean diurnal value:

$$(17.7 + 17.9 + 16.8 + 13.5)/4 = 16.5 \mu\text{mol s}^{-1} \text{ m}^{-2}.$$

Correcting to the whole summer mean values gives $16.5-0.1 = 16.4 \mu\text{mol s}^{-1} \text{ m}^{-2}$.

2. high aerosol loading, mean diurnal value: $(20.0 + 18.7 + 17.2 + 15.5)/4 = 17.9 \mu\text{mol s}^{-1} \text{ m}^{-2}$.

Correcting to the whole summer mean values gives $17.9-1.3 = 16.6 \mu\text{mol s}^{-1} \text{ m}^{-2}$.

Thus, the difference between mean diurnal values is $0.2/16.4 = 0.012 \approx 1.2\%$, which could be expected, as statistically significant difference in GPP of about 6% is there during two time slots, and part of that difference is compensated by the seasonal processes in the ecosystem.

The total GPP increase due to diffuse radiation effect in this ecosystem¹⁹ is 11% of the clear sky mean value or $1.7 \mu\text{mol s}^{-1} \text{ m}^{-2}$. Then a daily mean GPP increase found for high aerosol under cloudy sky constitute $0.2/1.7 \approx 12\%$ of the total average increase of photosynthesis possible for this ecosystem due to diffuse fertilization.

Estimates of the BVOC-photosynthesis feedback in boreal zone

To compare our photosynthesis results to those within the feedback simulated by Rap et al.²⁵, we first compare an increase in GPP. The increase in boreal zone simulated in this study in boreal zone was about $0.02\text{--}0.06 \text{ gC day}^{-1} \text{ m}^{-2}$

We first estimate an increase in GPP from our study in the same units as in Rap et al.²⁵:

$$0.2 \frac{\mu\text{mol CO}_2}{\text{m}^2 \text{s}} = 0.2 \cdot 10^{-6} \frac{\text{mol CO}_2}{\text{m}^2 \text{s}} = 0.2 \cdot 12 \cdot 10^{-6} \frac{\text{gC}}{\text{m}^2 \text{s}} = 0.2 \cdot 12 \cdot 60 \cdot 60 \cdot 24 \cdot 10^{-6} \frac{\text{gC}}{\text{m}^2 \text{day}} \approx 0.2 \frac{\text{gC}}{\text{m}^2 \text{day}}.$$

So our value is several times larger compared to that in Rap et al.²⁵. Note, however, that they reported an increase in GPP in response to 10% increase of BVOC emissions. Let's assume that 10% increase of emissions will lead to about 10% increase of BVOC concentration. Based on the median temperatures at low (ca 16°C) and high (ca 22°C) aerosol loading (Supplementary Fig. 7b), we can use Paasonen et al.⁷ monoterpene (MT) concentrations (their Supplementary Fig. 5b) to find how large increase we can get at these temperature difference:

$$\frac{[\text{MT}]_{22}}{[\text{MT}]_{16}} = \exp(0.09(22 - 16)) = 1.7 \quad (20)$$

This corresponds to increase in MT concentration of 70% compared to estimated 10% in Rap et al.²⁵ and suggests that if we want to compare increase in GPP in our system to the modeling study, we need to decrease it 7 times to get $0.2/7 = 0.03 \text{ gC day}^{-1} \text{ m}^{-2}$, within the range reported in this study ($0.02\text{--}0.06 \text{ gC day}^{-1} \text{ m}^{-2}$).

The latter estimate was obtained as follows. Note that cited study²⁵ quantified changes of different variables, not their absolute values. So we have to also quantify the change in GPP between the conditions with low and high aerosol loading to compare our results to that study. From our measurements-based estimates, we get:

$$\text{BVOC} = \text{BVOC}_0 + \Delta \text{BVOC} = 1.7 \text{BVOC}_0, \quad (21)$$

$$\text{GPP} = \text{GPP}_0 + \Delta \text{GPP} = \text{GPP}_0 + (0.2 \text{ gC day}^{-1} \text{ m}^{-2}). \quad (22)$$

Let GPP be a function of BVOC and other variables, so $\text{GPP} = f(\text{BVOC}, \dots)$. We assume that at least for the considered range of BVOC-GPP, a response of GPP to BVOC increase is linear, so that:

$$\text{GPP} = f(\text{BVOC}, \dots) = f(\text{BVOC}_0, \dots) + \frac{\partial f}{\partial \text{BVOC}} \bigg|_{\text{BVOC}_0} \Delta \text{BVOC} = \text{GPP}_0 + \Delta \text{GPP}. \quad (23)$$

Then, as $\text{GPP}_0 = f(\text{BVOC}_0, \dots)$ and $\frac{\partial f}{\partial \text{BVOC}} \bigg|_{\text{BVOC}_0} = \text{const} = \alpha$, for all the other parameters fixed:

$$\Delta \text{GPP} = \alpha \Delta \text{BVOC}. \quad (24)$$

From the latest equation, if we have results for 70% increase in BVOC and want to estimate an increase in photosynthesis for 10% increase in BVOC, then:

$$0.2 \text{ gC day}^{-1} \text{ m}^{-2} = \alpha 0.7 \text{BVOC}_0, \quad (25)$$

$$x \text{ gC day}^{-1} \text{ m}^{-2} = \alpha 0.1 \text{BVOC}_0 \quad (26)$$

$$\text{Then } x = \frac{0.2 \text{ gC day}^{-1} \text{ m}^{-2} \cdot \alpha 0.1 \text{BVOC}_0}{\alpha 0.7 \text{BVOC}_0} = \frac{0.2 \text{ gC day}^{-1} \text{ m}^{-2}}{7}. \quad (27)$$

Table 1 | Measured variables at SMEAR II used in the study

Variable	Unit	Measurement height
Temperature (T)	°C	16.8 m
Relative humidity (RH)	%	16.8 m
Cloud base height	m	—
Global radiation	W m ⁻²	18 m
Diffuse radiation	W m ⁻²	18 m
PAR	μmol m ⁻² s ⁻¹	18 m (2012–2017)/35 m (2017–)
Diffuse PAR	μmol m ⁻² s ⁻¹	18 m (2012–2017)/35 m (2017–)
Gross Primary Production (GPP)	μmol m ⁻² s ⁻¹	23 m
Organic Aerosol Mass	μmol m ⁻³	4 m

Further, we estimate the annual radiative effect due to increased photosynthesis uptake on the following assumptions:

25–50% of the days in summer are clear sky or cumulus clouds³⁰: 20–30% Cu clouds, 10–20% clear sky days, which would provide us the following minimum (maximum) annual uptake estimate:

minimum:

$$0.2 \frac{\text{gC}}{\text{m}^2 \text{day}} \cdot 90 \text{ days} \cdot 0.2 + 0.9 \frac{\text{gC}}{\text{m}^2 \text{day}} \cdot 90 \text{ days} \cdot 0.1 \\ = 3.6 + 8.1 = 11.7 \frac{\text{gC}}{\text{m}^2 \text{yr}};$$

maximum:

$$0.2 \frac{\text{gC}}{\text{m}^2 \text{day}} \cdot 90 \text{ days} \cdot 0.3 + 0.9 \frac{\text{gC}}{\text{m}^2 \text{day}} \cdot 90 \text{ days} \cdot 0.2 \\ = 5.4 + 16.2 = 21.6 \frac{\text{gC}}{\text{m}^2 \text{yr}}.$$

Then, following Joos et al.⁴⁴ and Bright et al.⁴⁵ we recalculate this annual carbon uptake into radiative effect (converting gC to gCO₂, 1 gC = 3.67 gCO₂):

$$\text{RF} = E \cdot A \cdot k_{\text{CO}_2} = -(11.7 - 21.6) \cdot 3.67 \cdot 10^{-3} \frac{\text{kg CO}_2}{\text{m}^2} \\ \cdot 0.5 \cdot 10^{15} \text{m}^2 \cdot 1.76 \cdot 10^{-15} \frac{\text{W}}{\text{m}^2 \text{kg CO}_2} = -(37.8 - 69.7) \cdot 10^{-3} \frac{\text{W}}{\text{m}^2} \\ \approx -(0.04 - 0.07) \frac{\text{W}}{\text{m}^2}, \quad (28)$$

where E is local annual CO₂-equivalent effect in [kgCO₂ m⁻²], A is the Earth surface area ($= 4\pi (6.4)^2 10^{12} \text{m}^2 = 0.5 \cdot 10^{15} \text{m}^2$) and $k_{\text{CO}_2} = 1.76 \times 10^{-15} \text{W m}^{-2} \text{kg CO}_2^{-1}$ is the radiative efficiency of CO₂.

The feedback strength can be obtained if we divide this radiative effect by 6.3 °C difference (Yli-Juuti et al.¹³), giving small negative feedback of $-(0.04 - 0.07) \frac{\text{W}}{\text{m}^2} / 6.3 \text{ °C} = -(0.006 - 0.011) \frac{\text{W}}{\text{m}^2 \text{ °C}}$ much smaller by absolute value than $-0.14 \frac{\text{W}}{\text{m}^2 \text{ °C}}$ reported by Yli-Juuti et al.¹³.

Data availability

Variables used in this study (listed in Table 1) are openly available at <https://smear.avaa.csc.fi/download> (under same names and measurement heights as in the table) besides organic aerosol mass, which was retrieved from the Source Data to Yli-Juuti et al.¹³ study. AERONET data (AOD₆₇₅) are available at <https://aeronet.gsfc.nasa.gov/>. The Source data for Figs. 1 and 2 is available from Zenodo repository: <https://doi.org/10.5281/zenodo.15745011>.

Code availability

The codes to make Figs. 1 and 2 from the Source data and to model diffuse radiation are available from Zenodo repository: <https://doi.org/10.5281/zenodo.15745011>.

Received: 22 January 2025; Accepted: 2 July 2025;

Published online: 23 July 2025

References

1. Betts, R. A. Offset of the potential carbon sink from boreal forestation by decreases in surface albedo. *Nature* **408**, 187–190 (2000).
2. Bonan, G. B. Forests and climate change: forcings, feedbacks, and the climate benefits. *Science* **320**, 1444–1449 (2008).
3. Hornberger, G. M., Wiberg, P. L., Raffensperger, J. P. & D'Odorico, P. *Elements of physical hydrology* (JHU Press, 2014).
4. Räty, M. et al. Dynamics of aerosol, humidity, and clouds in air masses travelling over Fennoscandian boreal forests. *Atmos. Chem. Phys.* **23**, 3779–3798 (2023).
5. Mäkelä, J. M. et al. Observations of ultrafine aerosol particle formation and growth in boreal forest. *Geophys. Res. Lett.* **24**, 1219–1222 (1997).
6. Kerminen, V.-M. et al. Atmospheric new particle formation and growth: review of field observations. *Environ. Res. Lett.* **13**, 103003 (2018).
7. Paasonen, P. et al. Warming-induced increase in aerosol number concentration likely to moderate climate change. *Nat. Geosci.* **6**, 438–442 (2013).
8. Tunved, P. et al. High natural aerosol loading over boreal forests. *Science* **312**, 261–263 (2006).
9. Kulmala, M. et al. On the mode-segregated aerosol particle number concentration load: contributions of primary and secondary particles in Hyytiälä and Nanjing. *Boreal Env. Res.* **21**, 319–331 (2016).
10. Teuling, A. J. et al. Observational evidence for cloud cover enhancement over western European forests. *Nat. Comm.* **8**, 14065 (2017).
11. Duveiller, G. et al. Revealing the widespread potential of forests to increase low level cloud cover. *Nat. Comm.* **12**, 4337 (2021).
12. Xu, R. et al. Contrasting impacts of forests on cloud cover based on satellite observations. *Nat. Comm.* **13**, 670 (2022).
13. Yli-Juuti, T. et al. Significance of the organic aerosol driven climate feedback in the boreal area. *Nat. Comm.* **12**, 5637 (2021).
14. Petäjä, T. et al. Influence of biogenic emissions from boreal forests on aerosol–cloud interactions. *Nat. Geosci.* **15**, 42–47 (2022).
15. Scott, C. E. et al. Substantial large-scale feedbacks between natural aerosols and climate. *Nat. Geosci.* **11**, 44–48 (2018).
16. Bonan, G. B. Forests, climate, and public policy: a 500-year interdisciplinary odyssey. *Annu. Rev. Ecol. Evol.* **47**, 97–121 (2016).
17. King, J. A. et al. Global and regional hydrological impacts of global forest expansion. *Biogeosciences* **21**, 3883–3902 (2024).
18. Blichner, S. M. et al. Process-evaluation of forest aerosol–cloud–climate feedback shows clear evidence from observations and large uncertainty in models. *Nat. Comm.* **15**, 969 (2024).
19. Ezhova, E. et al. Direct effect of aerosols on solar radiation and gross primary production in boreal and hemiboreal forests. *Atmos. Chem. Phys.* **18**, 17863–17881 (2018).
20. Gu, L. et al. Advantages of diffuse radiation for terrestrial ecosystem productivity. *J. Geophys. Res. Atmos.* **107**, 2–23 (2002).
21. Pedrúzco-Bagazgoitia, X. et al. Direct and Diffuse Radiation in the Shallow Cumulus–Vegetation System: Enhanced and Decreased Evapotranspiration Regimes. *J. Hydrometeorol.* **18**, 1731–1748 (2017).
22. Durand, M. et al. Diffuse solar radiation and canopy photosynthesis in a changing environment. *Agric. Meteorol.* **311**, 108684 (2021).
23. Neimane-Šroma, S., Durand, M., Lintunen, A., Aalto, J. & Robson, T. M. Sheding light on the increased carbon uptake by a boreal forest

under diffuse solar radiation across multiple scales. *Glob. Change Biol.* **30**, e17275 (2024).

24. Sporre, M. K., Blichner, S. M., Karset, I. H. H., Makkonen, R. & Berntsen, T. K. BVOC-aerosol-climate feedbacks investigated using NorESM. *Atmos. Chem. Phys.* **19**, 4763–4782 (2019).
25. Rap, A. et al. Enhanced global primary production by biogenic aerosol via diffuse radiation fertilization. *Nat. Geosci.* **11**, 640–644 (2018).
26. Kulmala, M. et al. A new feedback mechanism linking forests, aerosols, and climate. *Atmos. Chem. Phys.* **4**, 557–562 (2004).
27. Kulmala, M. et al. CO₂-induced terrestrial climate feedback mechanism: From carbon sink to aerosol source and back. *Boreal Env. Res.* **19B**, 122–131 (2014).
28. Artaxo, P. et al. Tropical and boreal forest-atmosphere interactions: a review. *Tellus B* **74**, 24–163 (2022).
29. Hari, P. & Kulmala, M. Station for measuring ecosystem-atmosphere relations (SMEAR II). *Boreal Env. Res.* **10**, 315–322 (2005).
30. Ylivinkka, I. et al. Clouds over Hyttiälä, Finland: an algorithm to classify clouds based on solar radiation and cloud base height measurements. *Atmos. Meas. Tech.* **13**, 5595–5619 (2020).
31. Eastman, R. & Warren, S. G. Diurnal cycles of cumulus, cumulonimbus, stratus, stratocumulus, and fog from surface observations over land and ocean. *J. Clim.* **27**, 2386–2404 (2014).
32. Heikkilä, L. et al. Long-term sub-micrometer aerosol chemical composition in the boreal forest: inter- and intra-annual variability. *Atmos. Chem. Phys.* **20**, 3151–3180 (2020).
33. Ineichen, P. A broadband simplified version of the Solis clear sky model. *Sol. Energy* **82**, 758–762 (2008).
34. Roderick, M. L., Farquhar, G. D., Berry, S. L. & Noble, I. R. On the direct effect of clouds and atmospheric particles on the productivity and structure of vegetation. *Oecologia* **129**, 21–30 (2001).
35. Bellouin, N. et al. Bounding global aerosol radiative forcing of climate change. *Rev. Geophys.* **58**, e2019RG000660 (2020).
36. Kohonen, K.-M. et al. Intercomparison of methods to estimate gross primary production based on CO₂ and COS flux measurements. *Biogeosciences* **19**, 4067–4088 (2022).
37. Ezhova, E. et al. Explainable machine learning for modelling of net ecosystem exchange in boreal forest. *Biogeosciences* **22**, 257–288 (2025).
38. Kulmala, M. et al. CarbonSink+ — accounting for multiple climate feedbacks from forests. *Boreal Env. Res.* **25**, 145–159 (2020).
39. Romps, D. M. Exact expression for the lifting condensation level. *J. Atmos. Sci.* **74**, 3891–3900 (2017).
40. Kulmala, L. et al. Inter-and intra-annual dynamics of photosynthesis differ between forest floor vegetation and tree canopy in a subarctic Scots pine stand. *Agric. Meteorol.* **271**, 1–11 (2019).
41. Launiainen, S. et al. Eddy covariance measurements of CO₂ and sensible and latent heat fluxes during a full year in a boreal pine forest trunk-space. *Boreal. Environ. Res.* **10**, 569–588 (2005).
42. Mahooti, M. NREL's Solar Position Algorithm (SPA), MATLAB Central File Exchange <https://www.mathworks.com/matlabcentral/fileexchange/59903-nrel-s-solar-position-algorithm-spa> (2024).
43. Holben, B. et al. AERONET – a federated instrument network and data archive for aerosol characterization. *Remote Sens. Environ.* **66**, 1–16 (1998).
44. Joos, F. et al. Carbon dioxide and climate impulse response functions for the computation of greenhouse gas metrics: a multi-model analysis. *Atmos. Chem. Phys.* **13**, 2793–2825 (2013).
45. Bright, R. M., Bogren, W., Bernier, P. & Astrup, R. Carbon-equivalent metrics for albedo changes in land management contexts: relevance of the time dimension. *Ecol. Appl.* **26**, 1868–1880 (2016).

Acknowledgements

This work was supported by ACCC (The Atmosphere and Climate Competence Center) Flagship funded by the Academy of Finland Grants No. 357902, 357903, 357904, 357905 (E.E., A.Aa, A.Ar, A.Lin, A.Lip, T.Y.J., H.K., I.Y., T.P., V.M.K., M.K., A.V.), Academy of Finland projects: 325681 (V.M.K.), 347780 (A.Lin, E.E., M.K.), 355142 (A.Lin), “Quantifying carbon sink, CarbonSink+ and their interaction with air quality” INAR project funded by Jane and Aatos Erkko Foundation (V.M.K., M.K.), Research Council of Finland competitive funding to strengthen university research profiles (PROFI) for the University of Eastern Finland (grant no. 352968) (A.V.), for the University of Helsinki (grant no. 353218) (A.Lin), Research Council of Finland research infrastructure funding (INAR RI) (T.P., M.K.), Horizon Europe programme under Grant Agreement No 101137680 via project CERTAINTY (Cloud-aERosol inTeractions & their impActS IN The earth sYstem) (H.K., A.V.), National duty funding to INAR (A.Aa, M.K.). University of Helsinki support via ACTRIS and ICOS funding is acknowledged. Support of the technical and scientific staff in Hyttiälä is gratefully acknowledged.

Author contributions

Conceptualization: E.E., A.V., M.K.; methodology: E.E., A.Ar, A.Lip, I.Y.; investigation: E.E., A.Aa; visualization: A.Aa, E.E.; interpretation of results: E.E., A.V., A.Ar, H.K., T.Y.J., A.Lin, T.P., M.K., V.M.K.; funding acquisition: H.K., A.V., A.Ar, T.P., E.E., A.Lin, M.K.; writing – original draft: E.E., A.Aa; writing – review & editing: A.Ar, A.Lip, A.Lin, H.K., I.Y., T.Y.J., T.P., V.M.K., A.V., M.K.

Competing interests

The authors declare no competing interests.

Additional information

Supplementary information The online version contains supplementary material available at <https://doi.org/10.1038/s43247-025-02539-z>.

Correspondence and requests for materials should be addressed to Ekaterina Ezhova.

Peer review information *Communications Earth & Environment* thanks Luciana Rizzo and the other, anonymous, reviewer(s) for their contribution to the peer review of this work. Primary Handling Editors: Nora Zannoni and Alice Drinkwater. [A peer review file is available].

Reprints and permissions information is available at <http://www.nature.com/reprints>

Publisher's note Springer Nature remains neutral with regard to jurisdictional claims in published maps and institutional affiliations.

Open Access This article is licensed under a Creative Commons Attribution 4.0 International License, which permits use, sharing, adaptation, distribution and reproduction in any medium or format, as long as you give appropriate credit to the original author(s) and the source, provide a link to the Creative Commons licence, and indicate if changes were made. The images or other third party material in this article are included in the article's Creative Commons licence, unless indicated otherwise in a credit line to the material. If material is not included in the article's Creative Commons licence and your intended use is not permitted by statutory regulation or exceeds the permitted use, you will need to obtain permission directly from the copyright holder. To view a copy of this licence, visit <http://creativecommons.org/licenses/by/4.0/>.

© The Author(s) 2025